Journal of Applied Mechanics and Technical Physics, Vol. 46, No. 6, pp. 773–779, 2005

COMPUTATIONAL MODELING OF THE STRUCTURE OF A HIGH-CURRENT DISCHARGE IN A MAGNETOGASDYNAMIC CHANNEL

E. N. Vasil'ev and D. A. Nesterov

UDC 533.95

A two-dimensional computational model is proposed to calculate radiative-convective heat transfer in gas flows with large gradients of physical properties. The model is based on the numerical solution of the unsteady dynamic equations for a compressible inviscid gas and the radiative transfer equations. Flow calculations for the magnetogasdynamic channel of a rail accelerator show that the dynamics of the process is substantially affected by the flow in the discharge region and hydrodynamic instability, resulting in the nonstationarity and nonuniformity of the flow and discharge structure. During the process, the discharge can exist both in the form of several current-carrying channels and in the form of a unified plasma formation. Results of the numerical calculations agree qualitative with experimental data.

Key words: *numerical modeling, magnetogasdynamics, discharge, rail accelerator, radiative-convective heat transfer.*

Introduction. Devices using high-current gas discharges are widely used in modern science and engineering. Such discharges are employed to heat gas in plasma generators, aerodynamic and shock tubes, magnetogasdynamic (MGD) generators and rail accelerators, and jet engines. The characteristics of MGD devices are largely determined by the structure of the discharge region formed during its interaction with magnetic field and gas flow. The efficiency of MGD interaction depends on a large number of parameters describing the working gas, gas-dynamic flow, external magnetic field, geometrical dimensions of the channel, and the external electric circuit. This paper deals with a numerical modeling of the formation of a high-current discharge under conditions of radiative-convective heat transfer as applied to rail accelerators.

Formulation of the Problem. We consider MGD interaction in the channel of the rail accelerator whose design and experimental results are described in [1]. The rail accelerator channel has a rectangular cross section, its top and bottom walls are formed by electrodes coupled to a current generator (long line), and its side walls are dielectric. The external-source energy heats a local gas region of the channel to a temperature that ensures thermal ionization. The current flowing through the discharge region sustains the conducting state of this region and compensates for radiative and convective energy losses. Because of the interaction of the current with the external transverse magnetic field, the conducting gas region is acted upon by an accelerating electrodynamic force, which causes the plasma region to move pushing the cold gas along the channel. In the experiment, the discharge current was 10–40 kA, the magnetic field 0.3–1 T, and the initial working-gas pressure 2.6–80 kPa.

The discharge structure was determined from simultaneous photographs of three views taken in the experiment. The following regularities in the formation of the high-current discharge structure were established.

1. After initiation, the cross section of the discharge core takes a stationary value, which as a rule is not more than 40–60% of the channel cross section.

2. After a transition process, the characteristic dimensions and the average discharge velocity varies weakly and the internal structure and shape of the current region are substantially unsteady.

Institute of Computational Modeling, Siberian Division, Russian Academy of Sciences, Krasnoyarsk 660036; ven@icm.krasn.ru; chief@vsptus.ru. Translated from Prikladnaya Mekhanika i Tekhnicheskaya Fizika, Vol. 46, No. 6, pp. 5–13, November–December, 2005. Original article submitted April 26, 2004; revision submitted March 3, 2005.

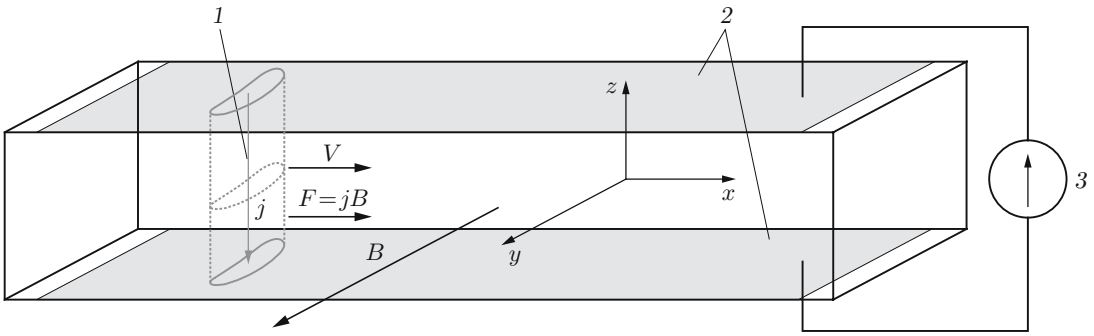

Fig. 1. Diagram of rail accelerator: 1) discharge; 2) electrodes; 3) current generator.

3. Separation of the discharge into several isolated current-carrying channels (in air and nitrogen, in 60 to 70% cases) or its complete destruction as a local formation are observed. In the last case, the current is distributed over almost the entire interelectrode gap of the rail accelerator.

In [1], it is stated that the physical reasons for the nonuniformity of the internal structure of the discharge and its destruction are not completely clear.

In the present paper, we study the physical mechanisms responsible for the formation of the discharge structure and flow in the rail accelerator channel. The process was modeled for air at an initial pressure close to atmospheric pressure; therefore, a magnetohydrodynamic approximation was used. In addition, for high-current discharges, the thermodynamic equilibrium condition [2] holds, and, hence, the degree of ionization, electrical conductivity, and other plasma properties can be expressed uniquely in terms of the thermodynamic parameters of the medium, for example, temperature and pressure.

In modeling the MGD interaction of the discharge, we consider the two-dimensional unsteady flow of an electrically conducting, radiating, inviscid gas in the middle cross section parallel to the electrode surface in a channel of constant width (Fig. 1). The characteristic parameters of the process are as follows: the current is $I = 2 \cdot 10^4$ A, the discharge velocity relative to the walls $u = 500$ m/sec, the radius of the conducting discharge column $R = 1.5$ cm, the induction of the external magnetic field $B = 0.6$ T, the gas temperature in the discharge $T = 10^4$ K, the electrical conductivity of the gas $\sigma = 3 \cdot 10^3\ \Omega^{-1} \cdot \mathrm{m}^{-1}$, the thermal conductivity $\lambda = 1\ \mathrm{W/(m \cdot K)}$ [3], and the Planck averaged absorption coefficient, $k_\mathrm{P} = 6.3\ \mathrm{m}^{-1}$ [4].

The numerical model includes three block: gas-dynamic, electrodynamic, and radiative. The gas flow in the channel is described by the two-dimensional equations of gas dynamics in Euler coordinates:

$$\frac{\partial \boldsymbol{U}}{\partial t} + \frac{\partial \boldsymbol{E}}{\partial x} + \frac{\partial \boldsymbol{F}}{\partial y} = \boldsymbol{S}; \tag{1}$$

$$\boldsymbol{U} = \begin{bmatrix} \rho \\ \rho u \\ \rho v \\ E_t \end{bmatrix}, \quad \boldsymbol{E} = \begin{bmatrix} \rho u \\ \rho u^2 + p \\ \rho uv \\ (E_t + p)u \end{bmatrix}, \quad \boldsymbol{F} = \begin{bmatrix} \rho v \\ \rho vu \\ \rho v^2 + p \\ (E_t + p)v \end{bmatrix}, \quad \boldsymbol{S} = \begin{bmatrix} 0 \\ f_x \\ f_y \\ Q + f_x u + f_y v \end{bmatrix}; \tag{2}$$

$$E_t = \rho((u^2 + v^2)/2 + e), \qquad p = p(\rho, e), \qquad T = T(\rho, e). \tag{3}$$

Here ρ is the gas density, u and v are the velocity components, p is the pressure, E_t is the total energy of a unit volume of the gas, e is the internal energy of a mass unit of the gas, T is the temperature of the gas, f_x and f_y are the components of the electrodynamic force acting on the gas along the x and y axes, respectively, and Q is the volumetric power of the energy sources and sinks.

In the problem considered, the volume variations of the energy due to radiative transfer Q_R and Joule dissipation Q_J are taken into account and the effect of heat conduction is ignored because of its smallness. Let us estimate the power of the heat-conduction mechanism using the quantity $Q_T = \lambda\, d^2T/dR^2 \approx \lambda\, \Delta T/R^2$ and the radiation power using the formula for an optically transparent medium $Q_R = 4k_\mathrm{P}\sigma_R T^4$. Here $\sigma_R = 5.67 \times 10^{-8}\ \mathrm{W/(m^2 \cdot K^4)}$ is the Stefan–Boltzmann constant. For the characteristic parameters of the process, we obtain

the values $Q_T \approx 4 \cdot 10^7$ W/m^3 and $Q_R \approx 10^{10}$ W/m^3. Calculating the radiative transfer for a flat layer under such conditions taking into account absorption, we obtain $Q_R \approx 10^9$ W/m^3 [5] for the temperature-gradient region.

For Eqs. (1)–(3), the initial conditions are the distributions of the temperature $T(x,y)|_{t=0} = T_0(x,y)$, pressure $p(x,y)|_{t=0} = p_0(x,y)$, and velocity $\boldsymbol{v}(x,y)|_{t=0} = 0$. The boundary conditions at the entrance to and on the side walls of the channel are defined as the conditions on an impenetrable wall using the method of mirror reflections. At the exit, we impose the conditions $\partial T(y,t)/\partial x|_{x=1} = 0$, $\partial p(y,t)/\partial x|_{x=L} = 0$, and $\partial v(y,t)/\partial x|_{x=L} = 0$, where L is the length of the channel.

In the experiments, the current value was determined by the external source; therefore, in describing the electrodynamic parameters in the numerical model, specified the time dependence of the current taking into account only the z-components of the electric-field strength and the current density. Let us estimate the magnetic Reynolds number $\mathrm{Re}_m = \mu_0 u \sigma \delta$, where the permeability of vacuum is $\mu_0 = 4\pi \cdot 10^{-7}$ H/m and $\delta = 2R$. Since $\mathrm{Re}_m \approx 0.06 \ll 1$, the model uses a noninductive approximation.

The magnetic field in the channel has two components:

$$\boldsymbol{B}(x,y) = \boldsymbol{B}_{\mathrm{ext}} + \boldsymbol{B}_{\mathrm{ind}}(x,y),$$

where $\boldsymbol{B}_{\mathrm{ext}} = (0, B_y, 0)$ is the constant external magnetic field and $\boldsymbol{B}_{\mathrm{ind}}$ is the magnetic field induced by the discharge. The value of the induced magnetic field $\boldsymbol{B}_{\mathrm{ind}}$ is estimated by the formula for a rectilinear infinite conductor:

$$B_{\mathrm{ind}} = \mu_0 I/(2\pi R) \approx 0.3 \text{ T}.$$

The obtained value is comparable with the external magnetic field; therefore, the effect of the induced magnetic field is taken into account in the rail accelerator model.

The electric-field strength in the discharge is the sum of the following components:

$$\boldsymbol{E} = \boldsymbol{E}_{\mathrm{ext}} + \boldsymbol{E}_{\mathrm{ind}} + \boldsymbol{v} \times \boldsymbol{B},$$

where $\boldsymbol{E}_{\mathrm{ext}}$ is produced by the external source and $\boldsymbol{E}_{\mathrm{ind}}$ is related to the nonstationarity of the induced magnetic field. Let us estimate the contribution of the terms in this expression for the characteristic parameters of the experiments $E_{\mathrm{ext}} \approx 10^4$ V/m, $\boldsymbol{v} \times \boldsymbol{B} \approx u B_{\mathrm{ext}} \approx 300$ V/m, and $E_{\mathrm{ind}} \approx B_{\mathrm{ind}} R/\tau_I \approx 50$ V/m ($\tau_I = 10^{-4}$ sec is the rise time of the current, and hence, of the magnetic field). The contribution of the terms $\boldsymbol{v} \times \boldsymbol{B}$ (3% of $\boldsymbol{E}_{\mathrm{ext}}$) and $\boldsymbol{E}_{\mathrm{ind}}$ (0.5% of $\boldsymbol{E}_{\mathrm{ext}}$) are small enough and their effects were ignored in modeling. The small value of $\boldsymbol{E}_{\mathrm{ind}}$ is additional support for the validity of using the noninductive approximation in the model.

The electromagnetic parameters were calculated from the discharge current value I and the current distribution $\sigma(x,y)$ using the relations

$$E = I \Big/ \iint \sigma(x,y)\, dx\, dy; \tag{4}$$

$$\boldsymbol{B}_{\mathrm{ind}}(x,y) = \frac{\mu_0}{2\pi} \iint\limits_S \frac{\boldsymbol{j}(x_1,y_1) \times \boldsymbol{r}}{r^2 \sqrt{1 + 4r^2/H^2}}\, dx_1\, dy_1; \tag{5}$$

$$j(x,y) = \sigma(x,y) E, \qquad Q_J(x,y) = j(x,y) E; \tag{6}$$

$$f_x = -jB_y; \qquad f_y = jB_x, \tag{7}$$

where E is the electric-field strength, $\boldsymbol{j} = (0,0,j)$ is the current-density vector, $\boldsymbol{r} = (x_1 - x, y_1 - y)$ is the radius-vector between the point of integration (x_1, y_1) and the point (x,y), $r = |\boldsymbol{r}|$, and H is the interelectrode gap.

The volume variation of the energy due to radiative transfer Q_R is calculated by solving the radiative transfer equations

$$\boldsymbol{a} \cdot \operatorname{grad} I_\nu = k_\nu (I_{\nu p} - I_\nu), \qquad \boldsymbol{W} = \int\limits_0^\infty d\nu \int \boldsymbol{a} I_\nu\, d\Omega, \qquad Q_R = \operatorname{div} \boldsymbol{W}, \tag{8}$$

where I_ν is the radiation intensity at a frequency ν, $I_{\nu p} = 2h\nu^3/[c^2(\exp\{h\nu/(kT)\} - 1)]$ is the equilibrium radiation intensity, $k_\nu(\nu, T, p)$ is the absorption coefficient, $\boldsymbol{a}$ is the unit vector in the photon flight direction, $\boldsymbol{W}$ is the radiation

energy flux, $h = 6.63 \cdot 10^{-34}$ J $\cdot$ sec is Planck's constant. The boundary conditions for Eqs. (8) are determined from the equality of the incident external radiation to zero: $I_\nu\Big|_\Gamma = 0$ (Γ is the boundary of the computational region).

Computational Algorithm. For each time layer, the numerical solution of Eqs. (1)–(8) includes three steps: the distribution of Q_R at each grid point is calculated from values of the temperature and pressure from the current time layer using Eqs. (8); the values of f_x, f_y, and Q_J and then the right sides of Eqs. (1)–(3) are calculated from the electrodynamic relations (4)–(7) and the electrical-conductivity distributions; the distributions of the physical parameters in the next time layer are obtained by solving the gas-dynamic equations (1)–(3).

In the first stage, the transfer equations are solved invoking a multigroup approximation; in this case, the entire frequency spectrum is divided into groups, in each of which the absorption coefficient is considered constant. The transfer equations are solved using the method of characteristics (the S_n-method) [6, 7]. Because this procedure takes most of the computation time, to reduce the time costs, we solve these equations only for the heated flow region and the nearest vicinity, where the radiation has a substantial effect on the process.

The gas-dynamic equations (1)–(3) are solved invoking an explicit McCormack scheme with splitting over the space coordinates [8]. This approach reduces the solution of the multidimensional problem to a successive solution of a set of one-dimensional problems. The flow contains regions with high gradients of physical parameters (the boundaries of the discharge and shock waves); therefore, to eliminate oscillations and increase the calculation accuracy, we employ the FCT-method for flow correction [9, 10].

A description of the computational algorithm for the gas-dynamic equations and the radiative transfer equation and results of test calculations are given in [5].

Data on the electrical conductivity and absorption coefficients of air are introduced into the program as tabular relations $\sigma(T, p)$ [3] and $k_\nu(\nu, T, p)$ [4].

Modeling Heat Transfer in the Rail Accelerator Channel. The process of discharge formation in the rail accelerator was calculated for a channel of width 6 cm and length 45 cm. For a spatial step of 3 mm, the number of nodes was 21×151. For the calculation of $\boldsymbol{B}_{\text{ind}}$, the height of the channel H was set equal to 5 cm.

Figure 2 and 3 give the results of flow modeling for the following parameters of the process: a gas temperature of $T = 300$ K, a pressure of $p = 80$ kPa, and an induction of the external magnetic field $B = 0.4$ T; the current value increases linearly from zero to 10 kA in 0.1 msec and then remains constant. The beginning of the computational experiment corresponds to the moment of formation of an initial current-carrying channel immediately after the breakdown of the interelectrode gap. According to this, a local high-temperature region in the shape of a rhombus (2×2 difference points) at a temperature of $1.2 \cdot 10^4$ K (Fig. 2a) was specified on the central axis of the computational region.

The passage of the current changes the power and energy balances in the discharge. The electrodynamic force causes the plasma region to accelerate and a pressure gradient is established in it (a shock wave propagates to the right and a rarefaction zone forms to the left of the discharge). In the beginning, when the discharge cross section is small and the current density is high, the discharge velocity was 1.1 km/sec ($t = 0.055$ msec). By the moment the discharge leaves the channel, the velocity decreased to 300 m/sec ($t = 1.4$ msec).

The variation in the discharge cross section is due to energy mechanisms. Joule dissipation provides energy supply to the discharge zone, and radiative heat transfer both limits the temperature rise and promotes the increase in the discharge cross section by heating of the cold gas in the nearest vicinity. By the time $t = 0.45$ msec, the discharge cross section overlaps more than half the channel width (Fig. 2b) and the temperature is approximately $2 \cdot 10^4$ K. Further increase in the discharge size is prevented by the circumfluous flow, which deforms the discharge region and carries away part of the heated gas from the edges.

Subsequently, the evolution of the interaction between the discharge and the flow becomes substantially unsteady (Fig. 2c, d, and e). At the leading edge, the discharge is subjected to the gas-dynamic pressure of the cold gas with a much higher density (the density ratio of the cold and heated gas is more than 50). A combination of these factors leads to the development of Rayleigh–Taylor hydrodynamic instabilities, because of which tongues of the denser medium penetrates into the lighter medium. The penetration of the cold gas into the plasma region separates parts of various dimensions from the discharge. The periodic development of the instability results in the formation of several discharge regions, which interact with the magnetic field and cold gas to form a vortical flow structure (see Fig. 3).

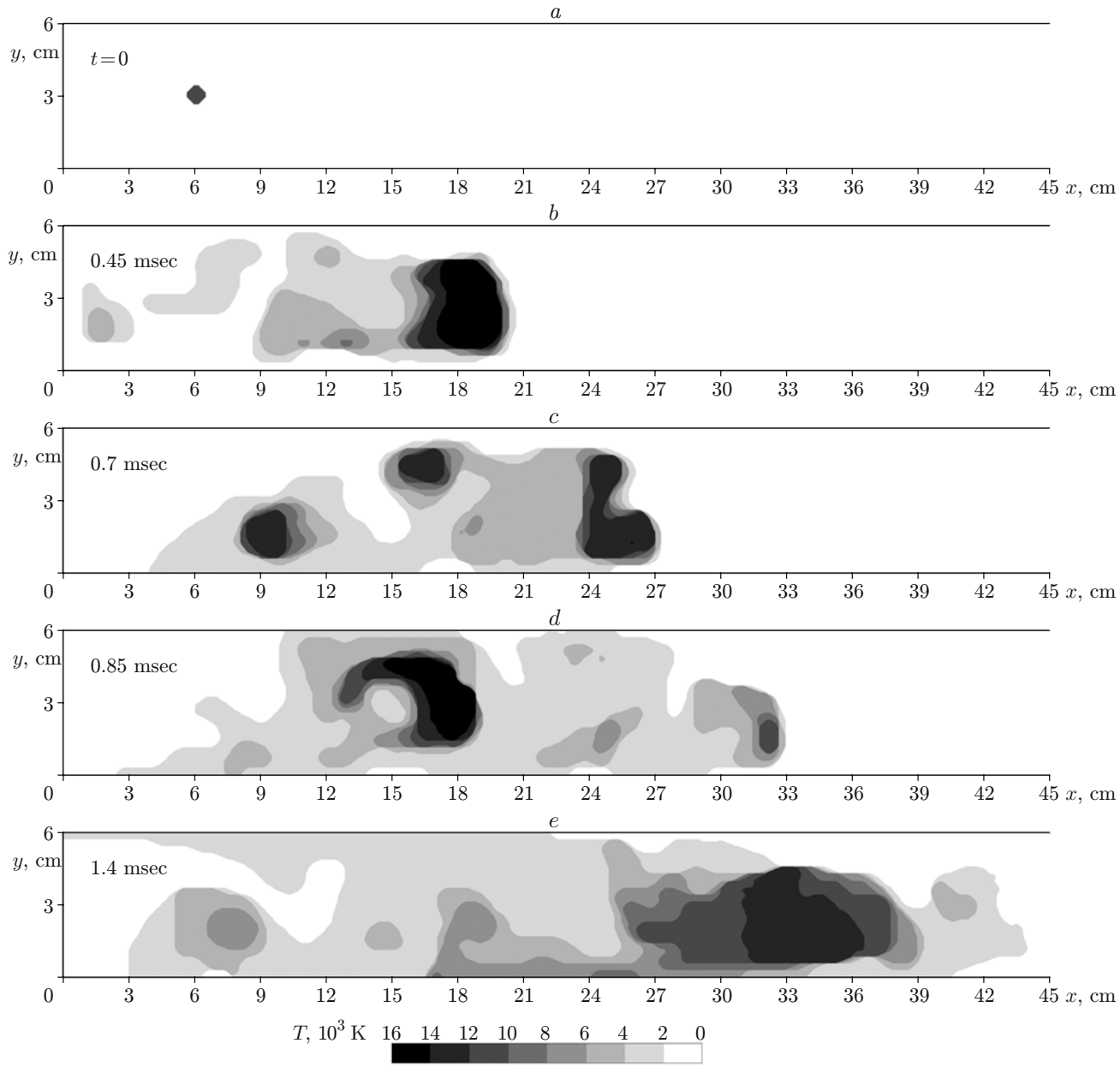

Fig. 2. Temperature distribution in the rail accelerator channel at various times for $I = 10$ kA, $p = 80$ kPa, and $B = 0.4$ T (the scale give the correspondence of tints of gray color to the temperature in 10^3 K).

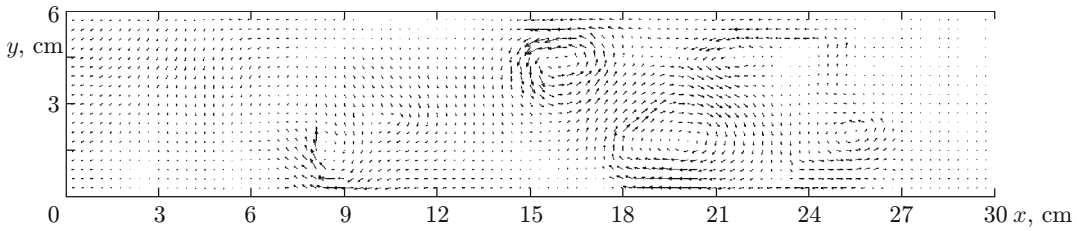

Fig. 3. Velocity field in the vicinity of the discharge (the parameters correspond to Fig. 2c).

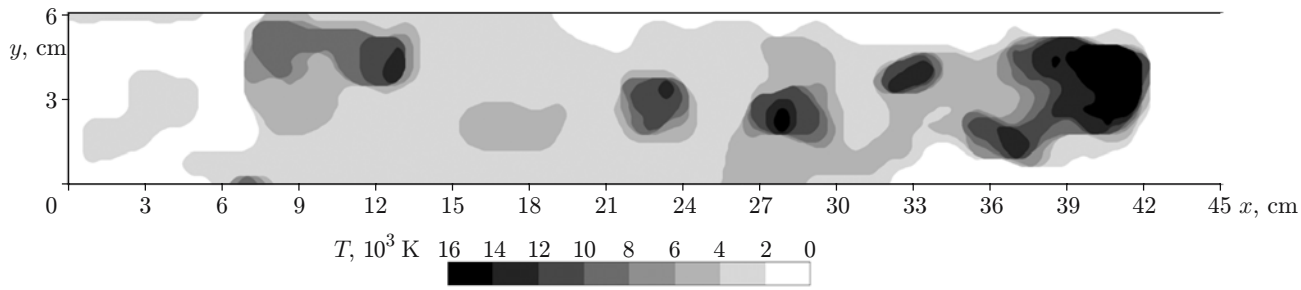

Fig. 4. Temperature distribution in the rail accelerator channel at $t = 0.72$ msec for $I = 20$ kA, $p = 80$ kPa, $B = 0.6$ T (the scale gives correspondence of tints of gray color to temperature in 10^3 K).

The evolution of each of the separated discharge regions is determined by the energy balance, primarily by the radiation, because the value of the radiative energy loss depends strongly on the discharge parameters. In particular, a pressure rise and a decrease in the cross-sectional size increase the energy loss. The conditions for the Joule dissipation vary to a lesser extent because of the weak dependence of the electrical conductivity on the pressure (at $T \approx 10^4$ K) and the uniformity of the potential distribution on the solid electrodes. In this regime, as long as the discharge head (leader) retained large sizes, the energy supply was high enough to maintain electrical conduction in it and the smaller discharge regions behind it gradually cooled down. By the time $t = 0.7$ msec after the separation of a number of small parts, the developed instability divided the leader into two parts similar in cross-sectional area (Fig. 2c). The combination of a high pressure and relatively small sizes resulted in cooling of both separated parts, because of which the total electric resistance of the gas in the channel, the potential difference in the interelectrode gap, and the current density in the other discharge regions increased. The current redistribution ensured heating and enlargement of the discharge region adjacent to the channel end, which was in the zone of the highest rarefaction and had the lowest radiative energy loss. This region began to increase in size and accelerate (Fig. 2d), but in contrast to the former leader, it moved over the perturbed gas. Therefore, because of interaction with vortices, its translational motion was accompanied by random displacements in the transverse direction. Therefore, at the exit from the channel, the discharge has a diffuse structure (Fig. 2e) with a maximum temperature of $T \approx 1.2 \cdot 10^4$ K.

From the calculation results, it should be noted that for symmetric initial and boundary conditions, the flow does not have marked deviations from rotational symmetry up to the time $t \approx 0.1$ msec, after which small fluctuations of the parameters due to rounding and approximation errors increase and violate the symmetry of the distribution of the physical parameters.

To study the effect of the initial conditions on the flow dynamics, we performed a computational experiment for the same process parameters but for the position of the initial electrically-conducting region shifted from the central axis of the channel by one computational interval (3 mm). Before the time $t = 0.6$ msec, this process was close in nature to the previous one. Subsequently, in the first regime, the leader separated into two parts and the flow structure changed radically. In the second case, the development of hydrodynamic instability resulted in separation of rather small parts from the discharge region during the entire process. These parts lagged behind the leader and gradually cooled down. In this case, the discharge head existed stably without significant shape and size changes, and its structure was similar to the configurations shown in Fig. 2b and d. In the regimes considered above, the Joule dissipation power was sufficient for the stable existence of only one discharge region.

The change in the process parameters in the rail accelerator affects both the average characteristics and the flow structure as a whole. An increase in the current intensity ($I = 20$ kA) and the external magnetic field induction ($B = 0.6$ T) at $p_0 = 80$ kPa also increases the nonuniformity of the discharge structure in the rail accelerator channel. The enhanced dynamic interaction causes many parts to separate from the main discharge region. In this case, the increased Joule dissipation power provides for the possibility of the simultaneous existence of several high-temperature discharge regions (Fig. 4), which are distributed over the entire length of the channel. In the this regime, the head discharge retained the largest cross section.

The numerical modeling of heat transfer in the rail accelerator channel showed that the process is characterized by substantial nonstationarity and nonuniformity of the flow. Furthermore, the formation dynamics of

the discharge structure in a two-dimensional formulation differs qualitatively from the process modeled in a one-dimensional approximation, where during the process of attainment of the energy and power balances, the discharge structure tends asymptotically to a stabilized state that hardly depends on the size of the initial perturbation and is completely determined by the initial flow parameters [11]. The qualitative difference in the nature of the processes is due to the limitations of the employed one-dimensional model, which does not adequately describe the flow processes and hydrodynamic instability.

In the regimes considered, discharge regions were formed in the form of both one local formation and several current-carrying channels, and the transition between these forms could occur even during the same process. This dynamics in the rail accelerator channel is due to the development of Rayleigh–Taylor hydrodynamic instability at the interface between gas regions of different density under the action of a body force. The instability developed under substantially unsteady conditions, and the vortical rotation of the gas in the plasma region, as a rule, shifts the zone of instability to the edge of the discharge. For this reason, a discontinuity of the discharge at the center was rarely observed in the modeling study and the size of the separated parts varied over wide ranges. The accelerator channel flow is unstable in the sense that small changes in the initial parameters or initial conditions can result in significant changes in the dynamics of the process.

The dynamics of the processes obtained using the computational model reflects the main experimental regularities in discharge formation in the rail accelerator channel. For a more detailed and quantitative comparison of the calculated and experimental results, the body of experimental data presented in [1] is insufficient.

REFERENCES

1. S. V. Kukhtetskii, V. A. Lyubochko, L. P. Mikhailenko, and K. V. Pertsev, "Integral model of a discharge in a rail accelerator taking into account circumfluous flow," *J. Appl. Mech. Tech. Phys.*, No. 1, 35–40 (1986).
2. Yu. P. Raizer, *Gas Discharge Physics* [in Russian], Nauka, Moscow (1987).
3. I. A. Sokolova, "Transport coefficients of air in the region of temperatures from 3000 to 25,000 K and a pressure of 0.1, 1, 10, and 100 atm," *J. Appl. Mech. Tech. Phys.*, No. 2, 213–221 (1973).
4. I. V. Avilova, L. M. Biberman, V. S. Vorob'ev, et al., *Optical Properties of Hot Air* [in Russian], Nauka, Moscow (1970).
5. E. N. Vasil'ev and D. A. Nesterov, "Numerical modeling of radiative-convective heat transfer for MGD flows with a T-layer," Institute of Computational Modeling, Krasnoyarsk (2004). Deposited at the VINITI 03.09.04, No. 399-V2004.
6. B. N. Chetverushkin, *Mathematical Modeling of Problems of Radiative-Gas Dynamics* [in Russian], Nauka, Moscow (1985).
7. V. N. Adrianov, "Grid method for studying radiative and complex heat transfer," *Izv. Akad. Nauk SSSR, Énerg. Transport*, No. 2, 142–150 (1988).
8. D. A. Anderson, J. C. Tennehill, R. H. Pletcher, *Computational Fluid Mechanics and Heat Transfer*, Hemisphere, New York (1984).
9. C. A. J. Fletcher, *Computational Techniques for Fluid Dynamics*, Springer-Verlag, Berlin–Heidelberg (1988)
10. D. L. Book, J. P. Boris, and K. Hain, "Flux-corrected transport. II. Generalization of the method," *J. Comput. Phys.*, No. 18, 248–283 (1975).
11. E. N. Vasil'ev, V. S. Slavin, and P. P. Tkachenko, "Sliding discharge stabilized by the walls of an MGD channel," *J. Appl. Mech. Tech. Phys.*, No. 4, 467–470 (1988).